Continental Shelf Research, Vol. 11, No. 3, pp. 269–293, 1991.
Printed in Great Britain.

0278–4343/91 $3.00 + 0.00

Fluid transport through Bass Strait

PETER G. BAINES,* GRAEME HUBBERT† and SCOTT POWER‡

(*Received* 20 *September* 1989; *in revised form* 18 *August* 1990; *accepted* 3 *November* 1990)

Abstract—The flux of water through Bass Strait was measured with two sections of current meter moorings placed in the west of Bass Strait between Cape Otway and King Island, and King Island and Hunter Island, in the autumn and winter of 1984. The flux was found to be highly correlated with the local wind stress and the time gauges on the northern boundary. Mean flux over the period of the experiment was 0.49 Sv from west to east, with a maximum of +3.05 Sv and a minimum of −0.8 Sv. Much of this flux occurred in surges lasting 2–3 days following the passage of atmospheric cold fronts across the region. The variations in flux may be monitored by a single tide gauge on the eastern Victorian coast, at least in winter. From dynamical considerations it is inferred from the available data that the through-flow is forced by a combination of forcing to the west of Bass Strait and wind stress within Bass Strait in the approximate ratio of 3:1. It seems probable that these surges are the principal cause of the coastally trapped waves observed in the Australian Coastal Experiment of 1983–1984 (H. J. FREELAND *et al.* (1986) The Australian Coastal Experiment: A search for coastal trapped waves. *Journal of Physical Oceanography*, **13**, 1230–1249). It appears that the geometry of Bass Strait causes singularities in linear coastally trapped wave theory in the south-west and north-east corners, and it is probable that this phenomenon is manifested in the stronger currents observed in the south-west than at the other stations further north.

1. INTRODUCTION

BASS Strait is located in the south-east corner of Australia, and separates Tasmania from the mainland. Its geometry is unique, in that it consists of a broad shallow region which descends abruptly to very deep water on two sides. The flux of water through Bass Strait and its variability are important quantities for a number of physical processes and applications in the region. These include the mean drift within the Strait and its possible effect on oil spills, etc., the transfer of water and associated material from the Bight region to the Tasman Sea and vice versa, and its effect on coastally trapped waves on the east Australian coast. It has generally been believed in the past that the net flow in winter is from west to east. NEWELL (1961) reported the motion of drift bottles which were released from Cape Northumberland and Cape Otway, and travelled eastwards through Bass Strait in winter, but not in summer. Their motion followed the direction of the prevailing winds in each season. Water mass analysis has also shown that high salinity water from the South Australian Gulfs is found (diluted) in Bass Strait, particularly in winter. Other observational studies which indirectly imply an eastward winter-time transport are those by GODFREY

*CSIRO Division Atmospheric Research, Aspendale, Australia.
†B.M.R.C. Bureau of Meteorology, Melbourne, Australia.
‡School of Mathematics, University of New South Wales, Australia.

et al. (1980) and TOMCZAK (1985). In this paper we present the first direct observations of the Bass Strait flux, and determine the factors causing it. The experiment was carried out in winter when the water column is known to be well mixed (BAINES and FANDRY, 1983); the results will not necessarily be applicable to summer when the winds are weaker and the water in the Strait stably stratified.

The flux was measured by deploying two sections of current meter moorings at the narrowest western entrances to Bass Strait. The northern section, from Cape Otway to Cape Wickham (King Island) consisted of four moorings (with two at the same location), each with two current meters, and the southern section, from King Island to Hunter Island, of two moorings. The general plan of the experiment was to integrate the currents through both sections to obtain the low-frequency flux as a function of time, and to correlate this time series with local wind and tide gauge records in order to determine the cause of the observed flux. Essentially, we aimed to determine whether the transport was directly forced by the local winds and atmospheric pressure gradient, or whether it was significantly forced by distant factors which manifested themselves in the surface elevation. Accordingly, data was collected from a number of tide gauges around Bass Strait (some deployed for the experiment) and from several wind stations maintained by the Bureau of Meteorology. The design of the experiment is described in Section 2, the observed currents, wind and tide gauge data in Sections 3 and 4, the interpretation and dynamical model linking these factors in Sections 5 and 6, and the conclusions are discussed in Section 7.

2. EXPERIMENTAL DESIGN

Two sections totalling six moorings were deployed with locations as shown in Fig. 1. The northern section from Cape Otway to King Island contained four moorings at three

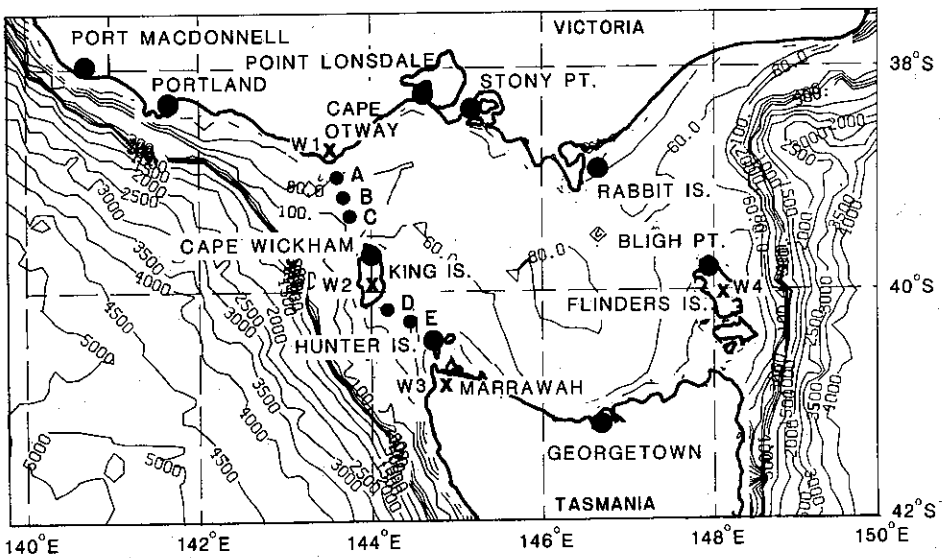

Fig. 1. Bass Strait, Showing the locations of the instruments used in the experiment. A, B, C, D and E refer to current meter moorings, W to wind stations, and the black circles denote tide gauge locations.

locations, A, B and C (with two moorings at the central site), and the southern section contained two moorings at locations D and E [at the central site of the northern section the two moorings (B1, B2) were deployed with a separation distance of ~2 km; for large-scale low-frequency motions, this represented a single mooring]. The locations and details of the instruments successfully recovered are shown in Fig. 2 and Table 1. Each Aanderaa current meter recorded the mean current speed and the instantaneous direction, temperature and pressure at 15 min intervals, and the Neil Browns gave a vector average of the same parameters over a 2-min interval every 20 min. The sections were designed to give optimum measure of the total fluid transport through both sections. The number of

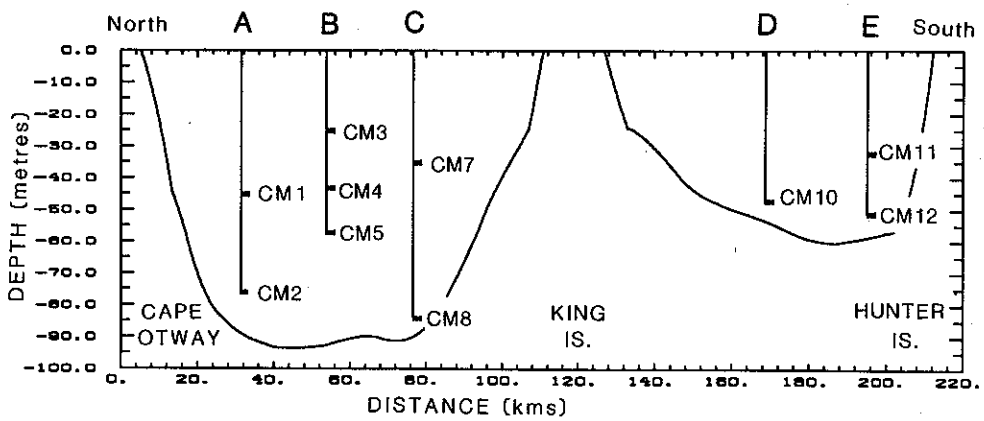

Fig. 2. Vertical cross-sections showing moorings and current meter depths and locations. The numbers denote instruments referred to in Table 1.

Table 1.

Current meter number	Type	Mooring	Location	Water depth	CM depth	Start	Record length (days)
1	Aanderaa	A	143°37.5′E	89	35	9/4/84 (EST)	88
2	Aanderaa	A	39°01.9′S	89	76	9/4/84	35
3	NB I	B1	39°12.9′S 143°44.1′E	95	25	9/4/84	54
4	NB I	B1	39°12.9′S 143°44.1′E	95	43	9/4/84	42
5	Aanderaa	B2	39°13.0′S 143°43.3′E	91	57	9/4/84	66
7	Aanderaa	C	39°24.2′S 143°50.7′E	97	35	8/4/84	88
8	Aanderaa	C	39°24.2′S 143°50.7′E	97	84	8/4/84	84
10	Aanderaa	D	40°12.3′S 144°11.2′E	60	47	7/4/84	82
11	Aanderaa	E	40°20.4′S	64	32	7/4/84	16
12	Aanderaa	E	144°26.9′E	60	51	7/4/84	75

moorings and the spacing between them was determined by the number of current meters available for the experiment, and it also depended on the assumption that the flow would not contain significant motion or eddies on the scale of the mooring separation or smaller. Such eddies were not expected because (i) the bathymetry is smooth, and (ii) the motion is barotropic at this time of year (see below), with deformation radius ~300 km. The assumption could be tested by examining the data, and was found to be justified. The Aanderaa current meters were located at depths of 30 m or greater, in order to minimize the corrupting effects of surface wave swell to which this instrument is susceptible.

The experiment was carried out in late autumn and winter, when Bass Strait is known to be neutrally stratified (BAINES and FANDRY, 1983), so that baroclinic effects due to vertical structure would be absent. Consequently, the velocity profile should be barotropic and a small number of current meters (i.e. two) would be sufficient to infer the mean velocity at one location. The four current meters (one failed) at the central northern moorings were designed to give a good description of the low-frequency velocity profile at this location, and it was assumed that the profile at other locations would be similar. Temperature data from these instruments and from CTD casts at the beginning and end of the experiment showed that the water column was very nearly neutrally stratified along both sections throughout the whole experiment.

Six sub-surface Aanderaa tide gauges were deployed at various locations around Bass Strait, of which only three were successfully recovered with a substantial record of data. These are denoted TG1–3 in Fig. 7, with their locations shown in Fig. 1. These observations were supplemented by data from five surface tide gauges and one sub-surface Aanderaa (Rabbit Island), maintained by State authorities and archived by the Tidal Laboratory of the Flinders Institute for Atmospheric and Marine Sciences. These are numbered TG4–9 in Fig. 7.

Wind and atmospheric pressure observations were obtained from four stations maintained by the Bureau of Meteorology which were known to produce reliable data. Three of these are located in a line in the west of Bass Strait, close to that of the moorings, at Cape Otway, Currie and Marrawah, and the other is on Flinders Island (see Fig. 1).

3. OBSERVATIONS OF CURRENTS AND FLUXES

The records from the current meters were divided into u and v components, where the u component was directed eastwards normal to the line of the section, and v was directed northwards along it. Means and trends were removed from the records for u and v, and they were then Fourier transformed. The dominant peak of the spectrum was centred on the semi-diurnal tides (EASTON, 1970; FANDRY *et al.*, 1985), with much smaller peaks at the diurnal tides and at low frequencies. Tidal energy exceeded the low-frequency energy by a factor of 10 or more, but the net tidal effect on transport was small because the tidal motion is periodic with zero mean. In every case, broad gaps with effectively zero energy separated the three regions of the frequency spectrum (semi-diurnal, diurnal and low-frequency), showing that the low-frequency motion with periods of 2 days or more was well separated from the higher-frequency tidal motion. The details of these low-frequency spectra vary from location to location, but they all have a dominant peak at about 0.11 cycles day^{-1}.

A filter proposed by THOMPSON (1983) which low-passed all periods greater than 2 days was applied to each time series. This filter is superior to a Godin filter, but the two were

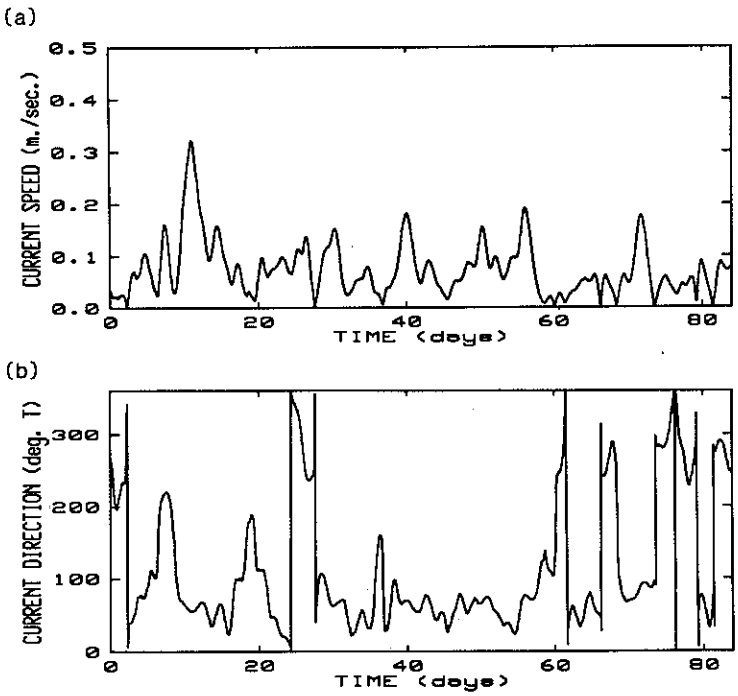

Fig. 3. Speed (a) and direction (b) of low-frequency filtered currents recorded by CM7 (see Fig. 2, Table 1). The time origin for this and other time series is 0000 UTC, 13 April 1984.

compared and found to give very similar results. The speed and direction for this low-passed record for CM7 is shown in Fig. 3. This record is again typical of the other instruments and some features should be noted. Firstly, the speed contains a number of salient peaks, separated at intervals of several days. Secondly, the flow is approximately bi-directional, alternating between a direction of 070° (i.e. near-eastward flow) and, less frequently, 266° (approximately). These directions lie approximately perpendicular to the section of moorings. Thirdly, for the most part the periods with high velocity occur when the direction is ~070°, and the velocity is low when the direction is ~266°. Expressing these velocities in u and v components (where u is perpendicular and v transverse to the section) shows, as would be expected, that u is somewhat larger than v, and the major surges in u are barely distinguishable in the v record.

All of the current meters show a remarkably similar pattern of variation, with coincident surges and bi-directionality. In general, for most instruments the u-velocities are larger and more coherent and the v-velocities are smaller (<5 cm s^{-1}) and relatively incoherent. The differences between the u components are small (Fig. 4). All of the major peaks in current velocity coincide, and each peak is present in every record. The direction of flow during these peaks is ~070°. There is a general decrease in fluid velocity with increasing depth of the instrument.

The similarity between the various moorings is demonstrated by an empirical orthogonal function analysis for the u components. Following KUNDU *et al.* (1975), the matrix of correlation coefficients for the eight current meters with longest simultaneous records (i.e.

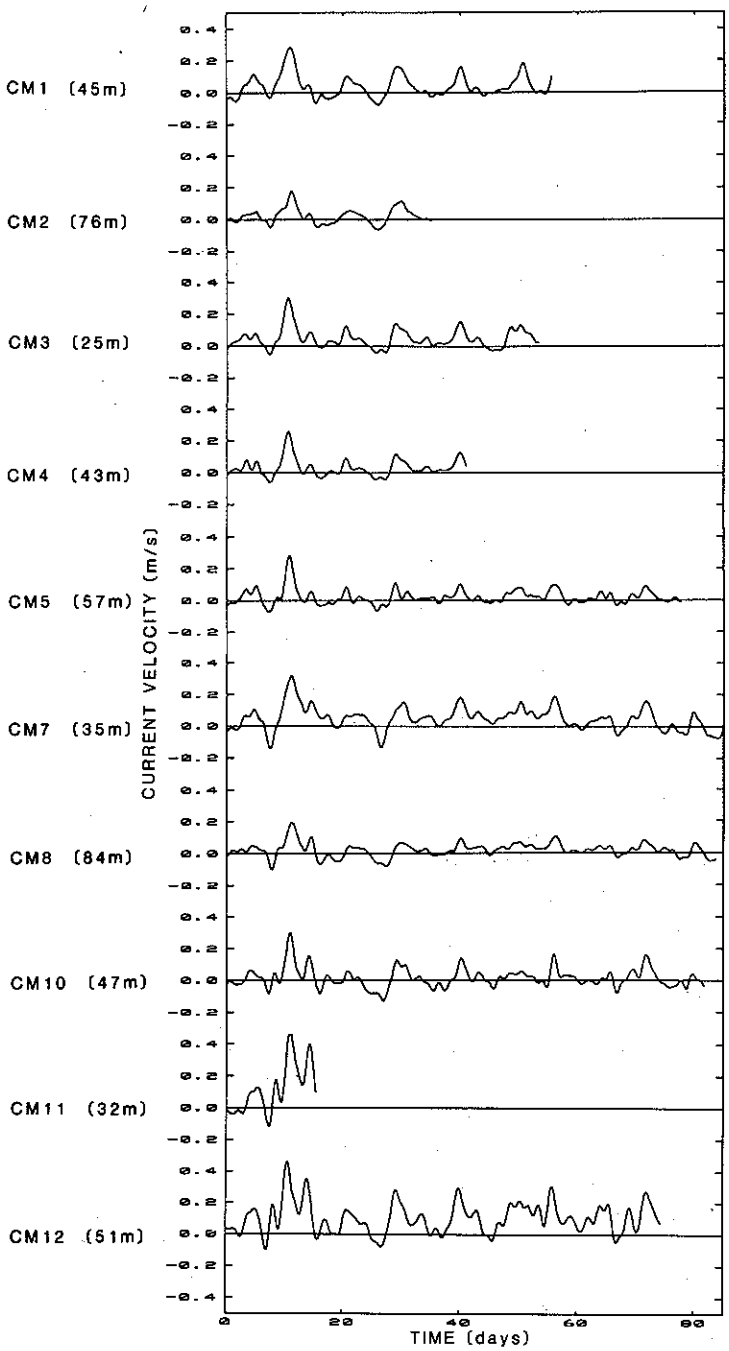

Fig. 4. Low-frequency filtered u-velocities for all 10 current meters in the two sections.

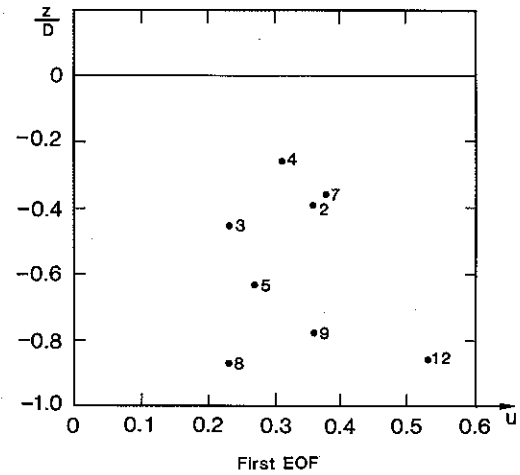

Fig. 5. Vertical profile of the low-frequency u-velocity from the first EOF, with the depth of each instrument plotted as a fraction of the local total depth.

excepting CM1 and CM11) was diagonalized to find the eigenvalues and eigenvectors. The first eigenvalue is found to account for 86% of the total (low-frequency) variance, with the second eigenvalue accounting for 5%. The relative values of the components of the first eigenvector are shown in Fig. 5, where the amplitude of the first EOF for each instrument is shown plotted with the instrument depth scaled with the local total depth. These also show a substantial degree of uniformity, except that the component at the southernmost mooring is significantly larger than all the others. It is clear from these results that the low-frequency flow pattern through these sections is quite simple and relatively uniform except, apparently, for the southernmost region. The u-velocity components were integrated across each section separately, using a mean profile in the vertical (from Fig. 5) and Simpson's rule along the section, to obtain the total fluxes as a function of time through each section. The fluxes are shown in Fig. 6, and each bears a general similarity to the u component of an individual instrument. For the northern section the flux varies between +1.8 and −0.5 Sv, with a mean (for the period 13 April–25 May) of 0.26 Sv. Results for the southern section are not as definite because of only three (and for the most part, two) current meters, although the coherence with the northern section gives confidence. For this section the flux (for the period 13 April–28 June) varies between +1.25 and −0.3 Sv, with a mean for the period of 0.23 Sv. Hence, the total flux varies (roughly) between +3.05 and −0.8 Sv, with a mean of +0.49 Sv. To summarize, the mass flux through Bass Strait in autumn and winter occurs mainly in surges of varying strength which may reach 2–3 Sv and last for 2 or 3 days, and which occur at intervals of about 6–9 days.

4. SEA LEVEL, WIND AND PRESSURE OBSERVATIONS

Data from the sub-surface tide gauges (TG1, 2, 3 and 9) were treated in a similar manner to those from the current meters. Spectral decomposition again showed a clear gap between the energetic tidal signals and the smaller low-frequency signals, and the latter were obtained by using the "Thompson" filter, giving the sub-surface pressure. The atmospheric pressure (taken from the nearest land station) was then removed from this to

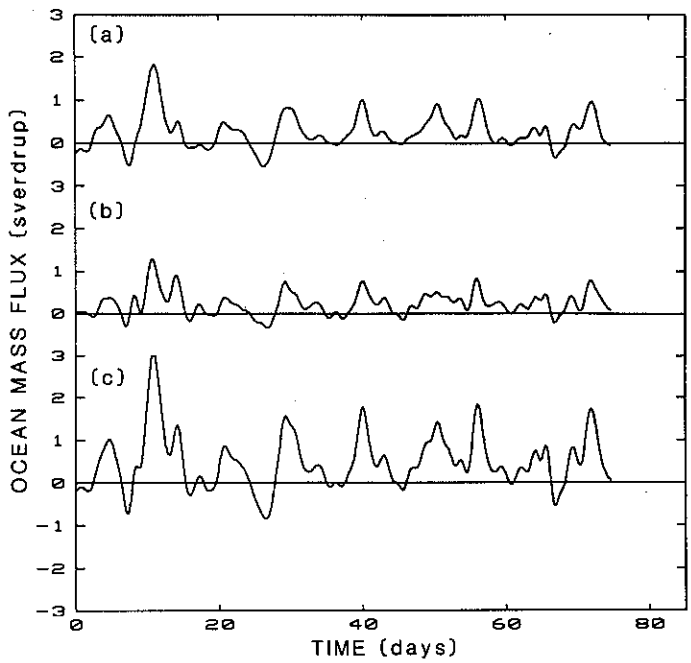

Fig. 6. Integrated flux through the northern section (a), the southern section (b) and their sum (c).

give the sea-surface elevation. Data from the remaining (surface) tide gauges were also low-frequency filtered. The sea-surface elevations were found to be more coherent than the sub-surface pressures, and we will employ the former in the following discussion. However, as discussed in Section 5, the sub-surface pressure is the dynamically more important quantity, as the sea level should respond as an "inverse barometer" at these frequencies.

The sub-surface tide gauges at Cape Wickham and Hunter Island, and to a lesser extent at Bligh Point, all shows a substantial increase in pressure early in the record (up to 0.7 m), with subsequent variations being small ($\sim \pm 0.05$ m). This large increase coincides with the first very strong current surge which is prominent in the records described in the previous section. The reason for it is not known, but its absence from the other tide gauge records suggests that it is due to dragging of the instruments to slightly deeper water, or current-induced settling of the instruments due to bottom stirring, or both. Accordingly, we disregard it in our subsequent interpretation of the events, and it has been removed from the curves of Fig. 7.

We present records of the sea-surface elevation in Fig. 7 for all nine instruments with a common time origin. Several features of this pattern of records may be noted. Firstly, the records on the northern continental boundary are all remarkably similar to each other and show a pattern of peaks which are generally very similar to those of the fluxes and u-velocity components described in the previous section, with which they are highly correlated with zero (or very small) lag. The amplitudes of the peaks generally increase towards the east. Secondly, the records from the tide gauges on the islands (TG 1, 3) and on the Tasmanian coast (TG 3, 8) are also similar but are significantly weaker. The record

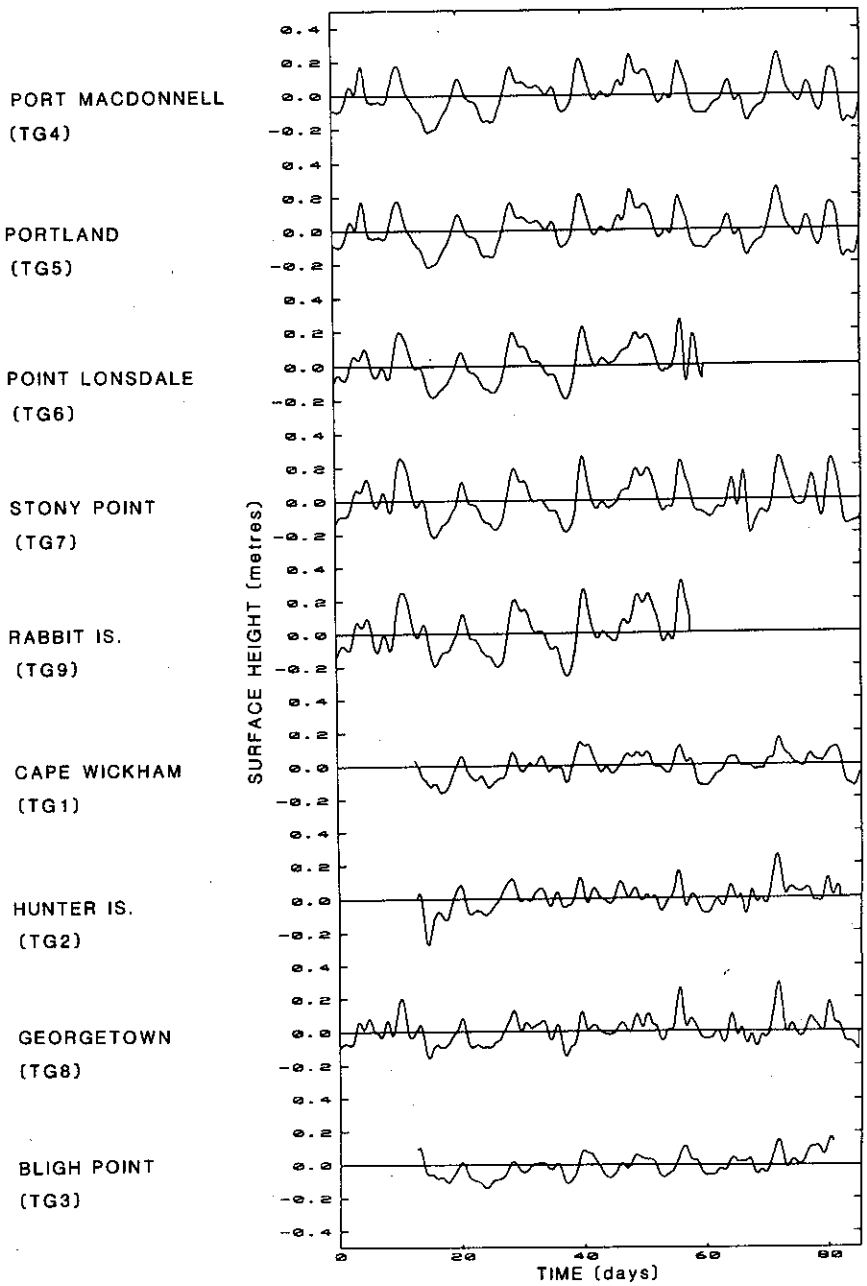

Fig. 7. Low-frequency filtered sea-surface elevations from all nine stations used in the experiment.

from Hunter Island contains more undulations than the others, and this will be commented on later.

Figure 8 shows the water temperature recorded by the Cape Wickham (TG 1) and Bligh Point (TG 3) instruments, which may be taken as the temperature of the local water

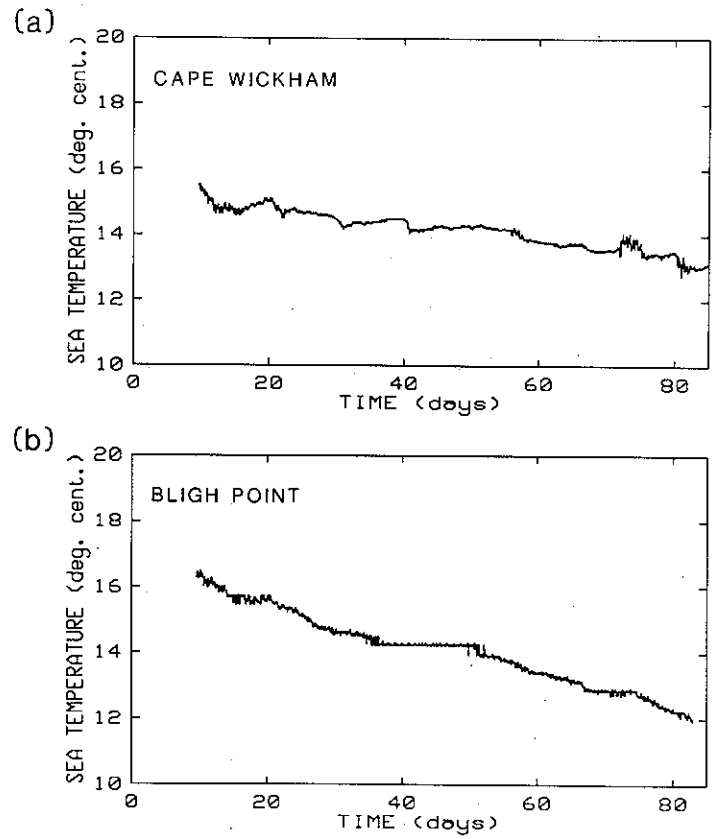

Fig. 8. Temperature records from (a) TG1 (Cape Wickham) and (b) TG3 (Bligh Point). The "flat" section in the centre of the Bligh Point record is presumably due to a temporary fault in the instrument.

column. The Cape Wickham record shows a net decrease in temperature with time, due to sudden falls interspersed with periods where the decline is gradual or near zero. The Hunter Island record has a similar character. The sudden falls are found to roughly coincide with the eastward surges in wind and current described above, and they have two possible causes—local cooling from the atmosphere, and advection. These are discussed in more detail in Section 7. At Bligh Point in the east, the periods of sudden fall in temperature are much less distinct than in the west.

The wind data were naturally noisier than those for the currents and pressures. North–south wind speeds were generally smaller, noisier and less well correlated with other variables than east–west winds. Nonetheless, data from the four stations showed a high degree of correlation between them (the mean of the 10 correlation coefficients between the four wind stations for east–west winds is 0.78). The mean eastward wind velocity observed at the five stations is shown in Fig. 9a (c.f. Figs 4 and 7), together with the total mass flux curve from Fig. 6. The most significant features of the wind records are surges lasting for several days. These are generally associated with south-westerly air streams following the passage of cold fronts across the region. Figure 10 shows the most prominent

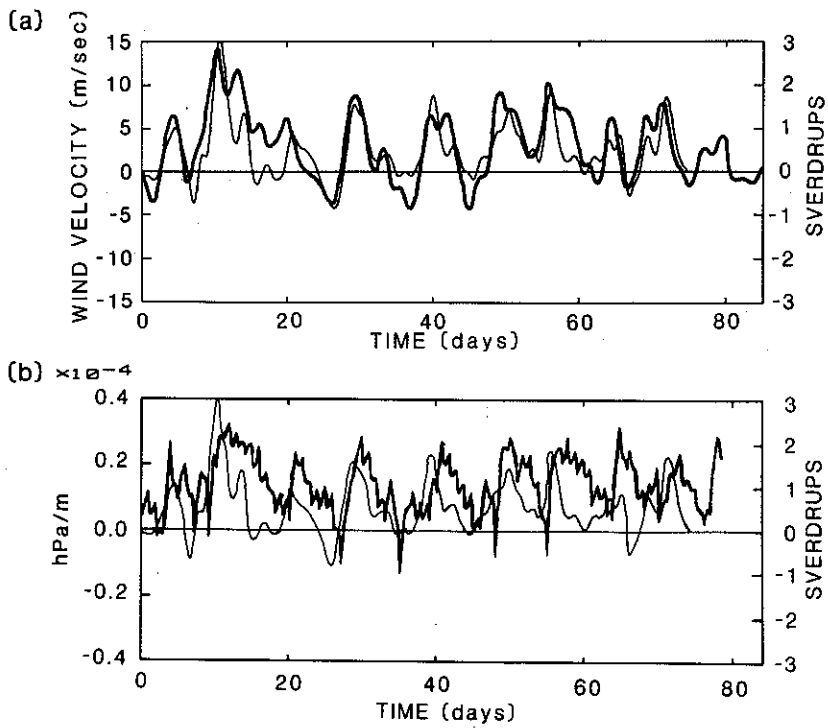

Fig. 9. (a) Eastward wind velocity averaged over the four stations (heavy curve), with the total mass flux (from Fig. 6c) superimposed (light curve). (b) North–south atmospheric pressure gradient, based on Stony Point minus Georgetown (heavy curve), compared with the total mass flux (light curve).

example, coinciding with the major surge early in the record. The north–south atmospheric pressure gradient (Stony Point minus Georgetown, Fig. 9b) was well correlated with the eastward wind velocity (correlation coefficient, $R = 0.85$) as expected from geostrophy, and with the oceanic mass flux ($R = 0.71$), but the east–west pressure gradient (Flinders Island minus King Island) was not well correlated with either.

5. THEORETICAL FRAMEWORK

The data described above show that the Bass Strait surges are closely related to local wind events, and it is tempting to conclude from Fig. 9 that the fluxes are directly forced by the local winds. However, the situation is not quite so simple, as a more detailed examination of the data shows.

The principal meteorological features of the region are cold fronts, followed by a south-westerly air stream, and separated by periods of several days with weaker winds; the latter tend to northerlies prior to the arrival of the next front. These eastward-travelling disturbances generate eastward-propagating coastally trapped waves (CTWs) on the Australian south coast wave-guide east of Cape Leeuwin (including the Bight region), which are manifested in sea level fluctuations (Provis and Radok, 1979; Church and

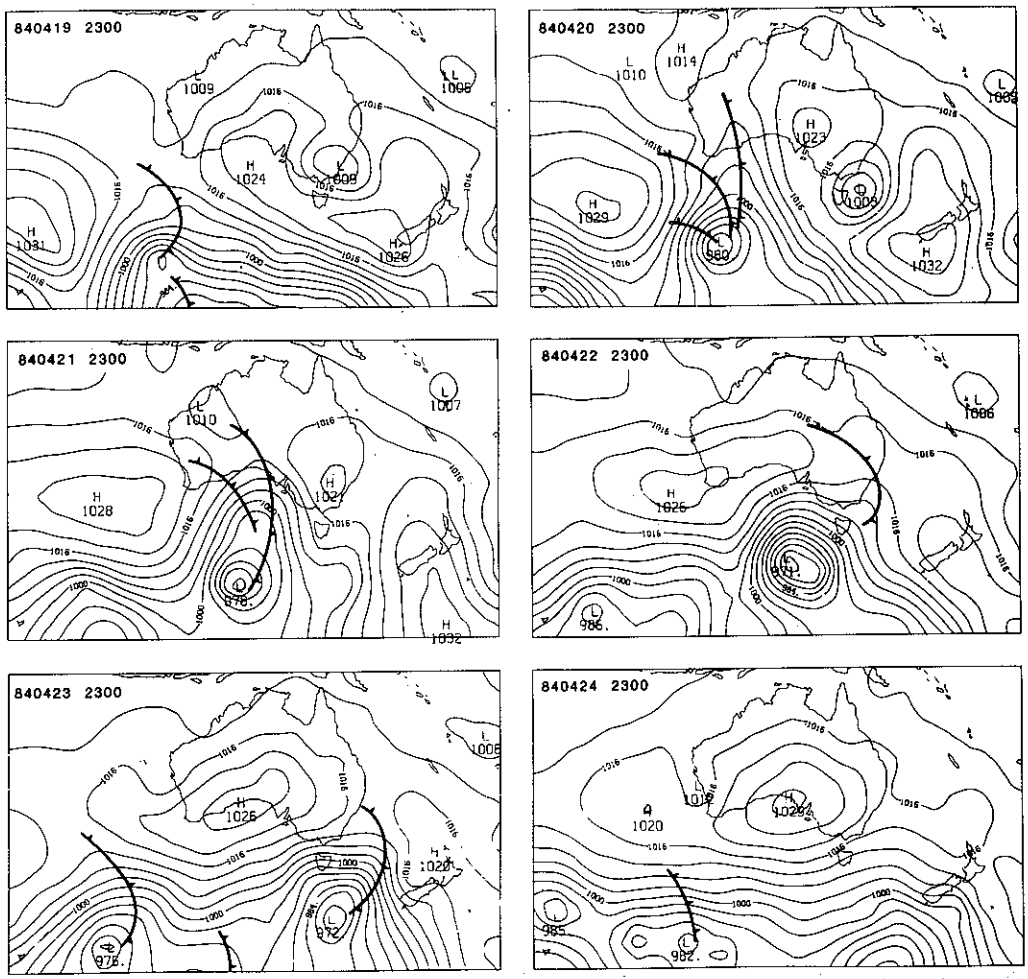

Fig. 10. Mean sea level atmospheric pressures at 2300 UT (0900 local time next day) for the period 19–24 April 1984, obtained from the Bureau of Meteorology.

FREELAND, 1987). Church and Freeland showed that these disturbances appeared to propagate through Bass Strait during the period of the ACE experiment, and the same behaviour is evident in the present data (compare, for example, the Portland and Stony Point tide gauge records, Fig. 7). Since the flow through Bass Strait is approximately geostrophic, these surges are coincident with the tide gauge fluctuations, and hence they may be related back to the waves generated in the Bight region, further west. We therefore have two possible causes for the Bass Strait flux, one caused by local atmospheric forcing and one caused by atmospheric forcing over an extensive region to the west. In order to determine the relative importance of these two causes, we must investigate the dynamics. We first give a general description of the dynamical phenomena involved, and then interpret the data within this framework in the next section. The dynamical models chosen are the simplest which are capable of describing the important aspects of the dynamics.

Coastally trapped wave generation

Eastward-directed wind stress over the ocean causes a northward Ekman transport in the Southern Hemisphere. The presence of the east–west coastline then forces the generation of CTWs in the coastal wave-guide. For the sake of this discussion we assume that the long wave theory of CTWs is applicable on the Australian south coast; this seems plausible, as the wavelength associated with meteorological forcing (≳2000 km) is much longer than the width of the coastal wave-guide. There are, however, substantial variations in the width of the continental shelf and slope along its length, and we must assume that the wave propagation is only determined by local properties. The long wave theory of CTW generation shows that the surface elevation, η_n, associated with a given mode, η_n, forced by the wind is governed by an equation of the form (e.g. GILL, 1982):

$$\frac{1}{c_n}\frac{\partial \eta_n}{\partial t} - \frac{\partial \eta_n}{\partial x} + R_n \eta_n = T_n(x,t), \tag{1}$$

where x is the coordinate along the coast, c_n is the wave speed of the nth mode, R_n is a frictional coefficient and $T_n(x,t)$ represents the projection of the x-directed component of the atmospheric forcing on this nth mode, whose cross-shelf structure will depend on the topography and density stratification. This forcing is primarily due to wind stress, but will also include atmospheric pressure effects. The general solution of this equation may be obtained by integrating along characteristics $s = t + x/c_n$, and if $\eta_n(x,t) = 0$ at $t = 0$, it has the form:

$$\eta_n(x,t) = -e^{R_n x} \int_{x+c_n t}^{x} e^{-R_n x'} T_n\left(x', \frac{x + c_n t - x'}{c_n}\right) dx'. \tag{2}$$

The travelling surges in the wind stress may be represented by a "top-hat" function moving eastwards at a speed c_w, so that

$$T_n(x,t) = \begin{matrix} T, (x - c_w t) < a, \\ 0, (x - c_w t) > a. \end{matrix} \tag{3}$$

Representative forms of the solution with $R_n = 0$ are shown in Fig. 11. Note that the system resonates if $c_w = c_n$. Generally, the forced sea level response lies between the wind-forcing region and the leading part of the travelling wave, regardless of which travels faster, so that this response may either lead the wind field or lag behind it. Values for c_w vary but a typical value is about 10 m s^{-1}. Speeds, c_1, of the lowest mode CTW are given by $c_1 \sim fl$, where l is the width of the continental slope region (GILL, 1982). This gives $c_1 \sim 16$ m s^{-1} in the Bight area where the slope is wide (CHURCH and FREELAND, 1987), and $c_1 \sim 3.5$ m s^{-1} on the Bonney coast where it is narrow, immediately to the west of Bass Strait. We might therefore expect the sea level response to lead the wind forcing in the Bight region, but the much slower propagation in the Bonney coast region means that the order may be reversed by the time the wave reaches Bass Strait. We may expect, therefore, that the wind forcing and the sea level response will arrive at Bass Strait at approximately the same time.

Behaviour of coastally trapped waves encountering Bass Strait

A simplified geometry of the western edge of Bass Strait is shown in Fig. 12. Coastally trapped waves approach from the west, and Bass Strait effectively acts as a very broad

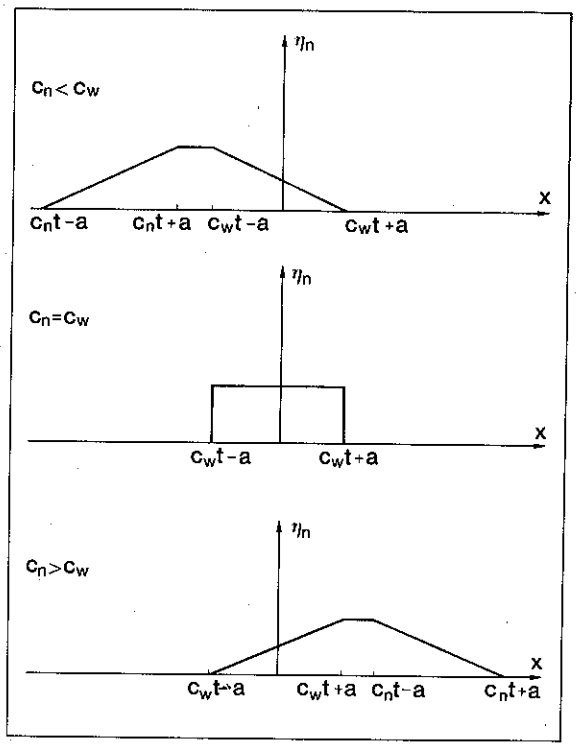

Fig. 11. Spatial variation of the amplitude of wind-forced CTWs when (a) wave speed is less than wind speed; (b) wave speed is equal to wind speed; (c) wave speed is greater than wind speed.

continental shelf. The changed structure of CTWs when the shallow strait is infinitely broad has been discussed by CLARKE (1987), who termed these waves "escarpment modes". The structure of the modes on the seaward (deep) side of the shelf break differs very little from that of the approaching CTWs. On the shallow side, however, the pressure perturbation at the shelf break is balanced by a Kelvin wave-like structure, so that the "escarpment mode" is a hybrid CTW–Kelvin wave.

In order to understand the behaviour of these modes it is convenient to consider the behaviour of a simpler model, or prototype, and the simplest prototype for this CTW–Kelvin wave hybrid is the double Kelvin wave, which propagates along a discontinuity in depth (LONGUET-HIGGINS, 1968). The inviscid behaviour of a Kelvin wave of low (effectively zero) frequency which encounters a discontinuous decrease in depth perpendicular to the coast has been discussed by GILL *et al.* (1986). Their analysis shows that when the incident Kelvin wave meets the depth discontinuity, it propagates offshore along it as a double Kelvin wave. On the shallow side, the shallow-water part of the double Kelvin wave then forces a Kelvin wave which propagates along the coast in the initial direction of motion of the incident deep-water Kelvin wave. In other words, the shallow-water Kelvin wave part of the double Kelvin wave turns the corner as shown in Fig. 12a, and propagates eastward along the Victorian coast. Further, the boundary condition of continuous pressure at the coast implies that the amplitude of the incident Kelvin wave, the transmitted Kelvin wave and the double Kelvin wave are all equal, as measured by the

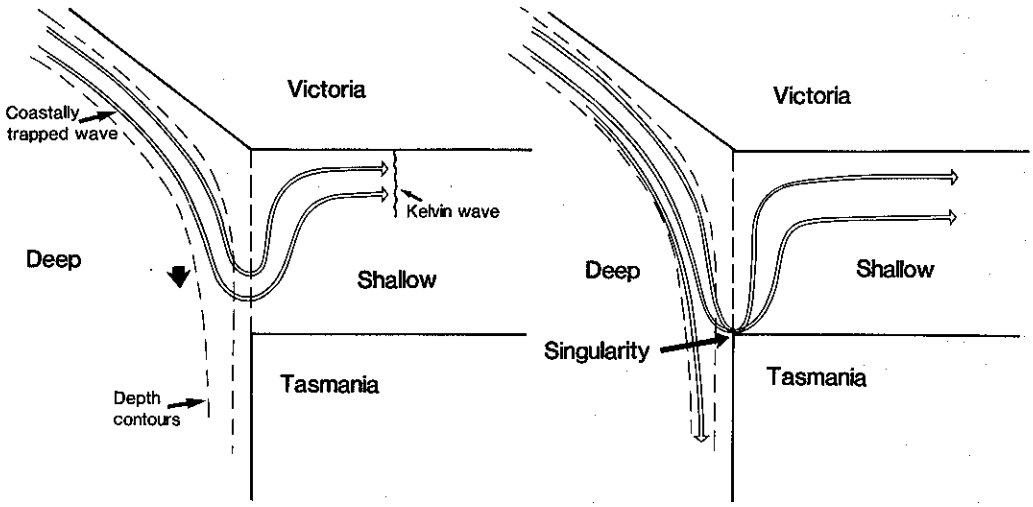

Fig. 12. Schematic diagrams of the splitting of wave energy of an incident CTW into a Kelvin wave moving across Bass Strait and an "escarpment mode". (a) Shows the wavefront propagating southward across the western entrance, and (b) the steady state established after the wavefronts have moved out of the picture.

pressure (free-surface elevation) at the coastlines and along the depth discontinuity. The incident Kelvin wave is therefore transmitted as one of the same amplitude (but less energy) into the shallow water.

By analogy, the same type of phenomena will apply if the incident wave is a CTW mode, rather than a Kelvin wave. Instead of double Kelvin waves, we have the escarpment modes described by CLARKE (1987), but the Kelvin wave behaviour on the shallow side will be the same. The energy flux of this Kelvin wave may be substantially less than that of the incident CTW, but, as shown below, it may be significant for the associated mass flux, and the dynamics within the Strait generally. CLARKE concluded that the energy flux entering and traversing Bass Strait is very small, but his analysis leading to this conclusion is incorrect. This is because the transmitted shallow-water Kelvin wave is not present in his analysis, because of inaccurate mathematical assumptions made in his Appendix B, leading to an erroneous equation (B11). His solution in fact corresponds to a sink of fluid at the Victorian coast, which absorbs the flux in the shallow-water Kelvin wave part of the escarpment mode.

If the incident CTW mode has the form of the sudden onset of a steady current, then flow across the depth discontinuity only occurs at the front of the disturbance, as is shown schematically in Fig. 12a. In the case of Bass Strait, this front propagates to Tasmania within a time scale of 1 or 2 days [the fastest mode has a speed of about 3.5 m s^{-1} (CLARKE, 1987)]. With geometry as shown in Fig. 12, the analysis of GILL *et al.* (1986) then shows that a singularity must develop where the depth discontinuity meets the coastline, where the flow across the step becomes infinitely large and narrow, as shown schematically in Fig. 12b. This implies that linear wave theory is unable to describe the flow in this region. The way in which friction and non-linear advection resolve this phenomenon is as yet

unknown. The actual geometry of the south-west corner of Bass Strait is only crudely approximated by Fig. 12, but the same dynamical processes should apply.

We may infer that low-frequency coastally trapped waves will enter Bass Strait as Kelvin waves with essentially the same amplitude, as measured by elevation at the coast, but that the mechanics of this transformation are not yet fully understood. That it nonetheless takes place is quite evident from the tide gauge records to the west of Bass Strait (Port McDonnell and Portland) and within it (Port Lonsdale, Stony Point and Rabbit Island) shown in Fig. 7.

As the Kelvin wave propagates across Bass Strait, its amplitude is reduced by bottom friction but the factor $\exp(-rx/cd)$, where r is the bottom friction coefficient, c the wave speed and d the depth, which gives an 11% reduction in amplitude in the distance $x = L$, using the values of the parameters given below.

Forcing within Bass Strait

We consider the effect of atmospheric factors acting on the water within Bass Strait alone. We assume a rectangular model geometry for Bass Strait of length L (east–west), width b, uniform depth d, and x, eastwards and y northwards with the origin at the north-west corner. Realistic values of the model parameters are: a length, L, of 460 km; width, b, of 260 km; and depth, d, of 70 m, with $f = -9.3 \times 10,^{-5}\ \mathrm{s}^{-1}$. This gives Kelvin wave speeds of about 26 m s^{-1}. Bottom friction is also important in such shallow water, and the bottom friction coefficient, r, is defined by

$$\tau_b = \rho_0 r \mathbf{u}, \tag{4}$$

where τ_b is the bottom stress, ρ_0 the fluid density and $\mathbf{u}$ the mean fluid velocity, and r has a typical value of 4.6×10^{-4} m s^{-1} [following CLARKE (1987)].

In order to calculate the effects of atmospheric forcing we employ the same model as CLARKE (1987). The equations of motion are

$$\begin{aligned}
\left(\frac{\partial}{\partial t} + \frac{r}{d}\right) u - fv &= -g \frac{\partial}{\partial x}(\eta + \eta_a) + \frac{\tau^x}{\rho_0 d}, \\
\left(\frac{\partial}{\partial t} + \frac{r}{d}\right) v + fu &= -g \frac{\partial}{\partial y}(\eta + \eta_a) + \frac{\tau^y}{\rho_0 d}, \\
\frac{\partial \eta}{\partial t} + d\left(\frac{\partial u}{\partial x} + \frac{\partial v}{\partial y}\right) &= 0,
\end{aligned} \tag{5}$$

where τ^x, τ^y denotes the wind stress, η_a denotes the atmospheric pressure in units of sea level elevation, and the boundary conditions are $v = 0$ at $y = 0, -b$. With $\tau^x \neq 0$, the forcing problem may be thought of as the generation of CTW motion on the northern boundary and separately on the southern boundary. On the northern boundary the CTWs lead the wind stress since $c_1 > c_w$, and on the southern boundary they do not since c_1 is negative. North–south wind stress, τ^y, results in an Ekman flux through Bass Strait which is not affected by the boundaries, and this will not be considered further here.

We considere the effect of an eastward wind stress only. Since cold fronts travel at about 10 m s^{-1}, the wind pattern crosses Bass Strait in about 12 h. Since we are primarily interested in the low-frequency response over several days, we may avoid discussion of the

details of the motion in the first few hours by making the following approximations. Firstly, we assume that the wind stress is uniform in space, and increases suddenly to a constant value at $t = 0$. Secondly, $\partial^2/\partial t^2 \ll f^2$, so that inertial oscillations are excluded, and thirdly, we make the long wave approximation ($\partial^2/\partial x^2 \ll \partial^2/\partial y^2$) of conventional CTW theory. Since we also have $r/d \ll |f|$, the problem for the wind-forced response reduces to

$$\left(\frac{\partial}{\partial t} + \frac{r}{d}\right)\frac{\partial^2 \eta}{\partial y^2} - \frac{f^2}{c^2}\frac{\partial \eta}{\partial t} = 0, \tag{6}$$

where $o^2 = gd$, and:

$$\frac{\partial \eta}{\partial x} - \frac{1}{f}\left(\frac{\partial}{\partial t} + \frac{r}{d}\right)\frac{\partial \eta}{\partial y} = \frac{\tau^x}{\rho_0 g d}(y = 0, -b). \tag{7}$$

The wind stress is given by

$$\begin{aligned} \tau^x &= 0, \qquad t < 0, \\ &T, \qquad t > 0 \end{aligned} \tag{8}$$

and the boundary conditions at the "ends", $x = 0, L$, are determined by the conditions of no inward-propagating energy.

The full solution of these equations is readily obtained but is needlessly complex for our purposes here, and we instead take the simpler course of obtaining the inviscid solution ($r = 0$), and the steady-state solution with $r \neq 0$.

With $r = 0$, the solution has the form

$$\eta = A(x,t)e^{y/\lambda} + B(x,t)e^{-y/\lambda}, \tag{9}$$

where $\lambda = c/|f|$. Following the procedure of CLARKE (1987), the conditions of no inward-propagating energy via Kelvin waves will be satisfied by

$$A(0,t) = 0, \qquad B(L,t) = 0. \tag{10}$$

This gives the solution

$$\eta = \frac{T}{\rho_0 g d}\left(\frac{xe^{y/\lambda}}{1 + e^{-b/\lambda}} + \frac{(x - L)e^{-y/\lambda}}{1 + e^{b/\lambda}}\right), (t > 0), \tag{11}$$

which is steady after the initial onset of the wind, as the development of the flow with the time due to Kelvin wave propagation has been compressed to an instant by the approximations made in obtaining equation (6).

With the drag term included ($r \neq 0$), this expression [equation (11)] describes the solution to equations (6)–(8) immediately after the initial onset of the wind. The flow then adjusts to a steady state under the influence of bottom friction in the time scale $t \sim d/r$. The condition of no incoming energy implies a symmetry in the solution, as exemplified in equation (11) in which

$$\eta(0,0) = \eta(L, -b), (\eta(L,0)) = -\eta(0,-b), \tag{12}$$

and with these conditions the steady-state solution to equation (6) for large times is

$$\eta = \frac{T}{\rho_0 g d}\frac{y + bx/L}{\dfrac{r}{|f|d} + b/L}. \tag{13}$$

Equations (11) and (13) both satisfy the condition $\eta_{xx} \ll \eta_{yy}$, and equation (13) gives a uniform velocity (approximately) of

$$u = \frac{T}{\rho_0 |f|} \frac{L}{bd} \frac{1}{(1 + rL/|f|bd)}, \tag{14}$$

throughout the region.

This model permits wave energy to propagate out of Bass Strait as Kelvin waves without affecting the nature of the flow in the interior. In fact, this is not correct, because the Kelvin wave flow from shallow to deeper water involves the same type of singular behaviour as discussed previously. This situation applies in the north-east corner of Bass Strait (near Gabo Island) as well as in the south-west corner. These "singularities" render this dynamical description somewhat incomplete, but it is reasonable to assume that they only affect the flow locally, and do not alter the overall picture described by the linear equations.

Some of the principal features of these solutions, equations (11) and (14), may be seen in the numerical studies of FANDRY (1982) with wind-driven flow through Bass Strait with realistic topography. The comparison is far from perfect, however. In the numerical solutions there is wind forcing outside the Strait as well as inside, the wind directions used do not correspond well, and there are problems with the boundary conditions, particularly in the east. However, the solutions shown in Figs 5 (c,d) and 6 (c,d) of FANDRY (1982) show a similar pattern for the sea level elevation to that of the above equations, and appear to give a numerical manifestation of the flow in the regions of the singularities mentioned above.

The eastward wind is well correlated with the north–south atmospheric pressure gradient (correlation coefficient, 0.85), so that the two factors may be regarded as co-existing together. An analysis of the dynamical response of the Bass Strait geometry to an imposed north–south pressure gradient $d\eta_a/dy$ via equation (5) indicates that, for these low-frequency motions, the response should be predominantly that of an "inverse barometer", i.e. $\eta = -\eta_a$. Since $d\eta_a/dy > 0$ for an eastward wind, this causes a depression of the sea level in the north and an elevation in the south, with the dynamically significant quantity being $\eta + \eta_a$, the sub-surface pressure. We will consider the effect of $d\eta_a/dy$ as a separate entity, bearing in mind that it is a surrogate for a difference in sea level elevations.

On the basis of the above discussion, we may infer that the wave energy entering Bass Strait is given by the amplitude of the coastal sub-surface pressure variations $(\eta + \eta_a)$ in the north-west corner. On encountering Bass Strait the energy of CTWs from the west splits into two wave guides—one carrying Kelvin waves in Bass Strait, and the other CTWs propagating down the west coast of Tasmania. Of these two, the latter probably contains the larger proportion of energy flux. The energy in the Kelvin wave is determined by the amplitude at the coast, which is continuous with that of the incident (low frequency) CTW. The associated energy flux through Bass Strait due to these waves can therefore be readily calculated, and is given by (e.g. CLARKE, 1987)

$$E_{\text{flux}} = \frac{\rho_0 d g^2}{2|f|} \overline{\eta_0^2} (1 - e^{-2b/\lambda}), \tag{15}$$

where η_0 is the sub-surface pressure of the Kelvin wave in the north-west corner and $\overline{\eta_0^2}$ its mean-square value. The associated volume flux at any given time in this Kelvin wave is given by

$$M_1 = \frac{gd}{|f|}\eta_0(1-e^{-b/\lambda}), \tag{16}$$

across the western entrance to Bass Strait.

On the other hand, the flow forced by the wind in Bass Strait is related to the downward depression of the free surface in the south-west corner, or the change in elevation at the coast from east to west (on either coast). The total volume flux obtained from equation (11) for the inviscid case is

$$M_2 = \frac{TL}{\rho_0|f|}\frac{1-e^{-b/\lambda}}{1+e^{-b/\lambda}}, \tag{17}$$

and for the steady state with bottom friction the mass flux is

$$M_3 = \frac{TL}{\rho_0|f|}\frac{1}{1+rL/|f|db}. \tag{18}$$

With the values of the parameters given above we have $rL/|f|bd = 0.13$, $b/\lambda = 0.93$, so that $M_2, M_3 < TL/|f|\rho_0$.

In a sense, obviously, this division of the sources of the Bass Strait mass flux into generation inside and outside Bass Strait is artificial, because the process is essentially a continuous one.

6. COMPARISONS AND CAUSES

We may now employ the theoretical framework of the preceding section to interpret the current and tide gauge data. A principal hypothesis in this interpretation is that the current through Bass Strait is in geostrophic balance. That this is at least approximately true is shown in Fig. 13, where the total flux is shown plotted against the sea level elevation at Rabbit Island (TG 9). The correlation coefficient is 0.89, which is the largest for all the tide gauges on the northern boundary. This implies that a single tide gauge on the Victorian coast may be used to give a reliable estimate of the variation of the flow through Bass Strait, at least in winter. A relation between flux and sea level elevation obtained from Fig. 13 is

$$M = (0.49 + 5.98\,\eta_0) \times 10^6\ \mathrm{m^3\,s^{-1}}, \tag{19}$$

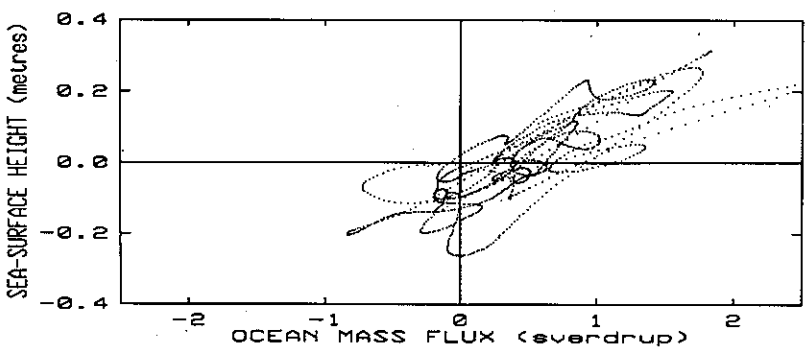

Fig. 13. Sea-surface height at Rabbit Island plotted against total mass flux; each point denotes a 12 h period.

with η_0 expressed in metres, where zero elevation corresponds to the mean flow.

From the preceding section, we may assume that the effects of coastally trapped waves generated along the Australian south coast (west of Bass Strait) on the flow in Bass Strait are described by tide gauges at the north-west corner. We will choose the tide gauge at Portland (the most appropriate location) to describe this externally forced flow within Bass Strait, via equation (16). The propagation of a wave into Bass Strait as a Kelvin wave of the same amplitude causes the sea level to rise or fall in phase on both the northern and southern coasts, with of course a much smaller amplitude (by a factor of 0.39) on the Tasmanian coast because of the exponential decay, cf. wind effects via equations (11) and (13).

A comparison between the observed flux and the inferred flux from the tide gauges at Portland and Rabbit Island, connected by equation (16) is shown in Fig. 14. For simplicity, only the principal corresponding peaks and troughs of each curve are shown. The mean flux (0.49 Sv) has been removed from the flux curve, so that all three curves refer to variations about their mean values. If we consider the ratio of the flux inferred from Portland to the observed flux of Fig. 14 for each of the nine peaks, we obtain the mean value of 0.63. This implies that 63% of the variation in the peak flows is due to forcing to the west of Bass Strait (and this is in fact a slight underestimate, since Portland is a little to the west of the Bass Strait entrance). This leaves 37% to be accounted for by other means, namely atmospheric pressure, and wind forcing within Bass Strait.

The peaks of the Rabbit Island curve in Fig. 14 do not coincide with those of the "flux" curve, the ratio of Rabbit Island flux to observed flux for these seven peaks being only 0.67. We may attribute this to the following reasons. Firstly, Rabbit Island is not at the

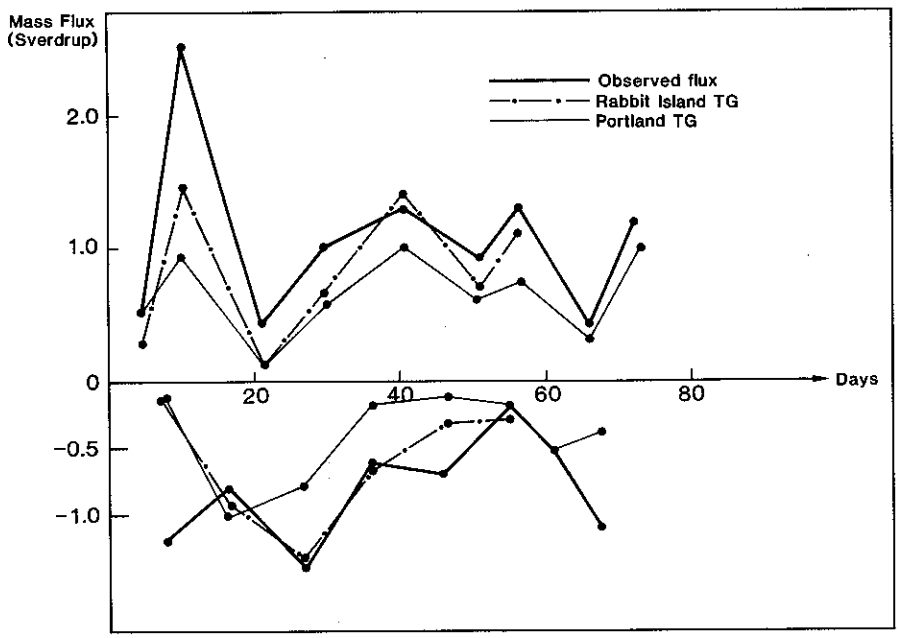

Fig. 14. Peaks and troughs of the curves of observed total mass flux with the mean (0.49 Sv) removed, and sea level at Portland and Rabbit Island, converted to mass flux units via equation (16).

eastern end and has $x/L = 0.7$ (see Fig. 1), whereas we require $x/L = 1$. Secondly, from the preceding section, dissipation will reduce the incoming Kelvin wave amplitude as it propagates across Bass Strait, making the mass flux more uniform with latitude. Thirdly, we have the effect of the north–south atmospheric pressure gradient. From Fig. 9(b), during peak flows this is approximately uniform at ~6 mb/260 km, with an overall mean of 3 mb/260 km. Equating 3 mb to 3 cm of surface elevation, from equation (16) this is equivalent to 0.13 Sv, which is, on average, 89.5% of the peak fluxes.

Given these complications, one is inclined to accept the incoming flux at Portland as the most reliably estimated of these quantities, so that, in round numbers, the contributions to the variation in the total flux from the forcing to the west of Bass Strait and the forcing inside Bass Strait are taken to be in the ratio 65:35.

For the southern tide gauges, the data from Cape Wickham (TG1) and Bligh Point (TG3) are similar to those of the north coast stations but with reduced amplitude, as expected from the theoretical interpretation of the preceding section. The Hunter Island record (TG2) is also of modest amplitude but is more complex. On the basis of the previous section one is tempted to interpret this as being due to a partial cancellation of the incident Kelvin wave and the wind-forced response (where eastward wind stress depresses the local sea level), where these factors are out of phase. Geogetown (TG8) has larger amplitudes, which is consistent with this interpretation.

The local effect of the wind on the flux may be estimated from the data in two ways. Firstly, by the change in surface elevation on the northern boundary from west to east, where (neglecting bottom friction) this contribution to the total flux may be regarded as due to the increasing amplitude of a Kelvin wave, and is given by equation (16), with η_0 representing this height difference. The *total* flux is therefore given by the height at the north-east corner. Secondly, the local wind-driven flux may be obtained directly from the wind by equation (17) or (18). From Fig. 9a, the wind speed during the peak flows, averaged over the five stations, is about 6 m s^{-1}, which implies a wind stress of about 0.1 N m^{-2}. From equations (17) and (18) this gives $M_2 = 0.21$ Sv and $M_3 = 0.44$ Sv, for the mean volume flux in the peaks. This is generally consistent with the above estimates from the tide gauges, that the local winds contribute about 35% of the total flux.

We may also use the wind, current and tide gauge data to obtain estimates of the energy budget within Bass Strait. From equation (5), we may derive the energy balance equation:

$$\frac{\partial}{\partial t}\frac{1}{2}\int (\mathrm{d}u^2 + g\eta^2)\mathrm{d}A = \frac{1}{\rho_0}\int u(\tau_w - \tau_b)\mathrm{d}A$$

$$T_w - T_b$$

$$- g\int \eta \mathrm{d}u \cdot ds + (-g)\int \mathrm{d}u \cdot \nabla\eta_a \mathrm{d}A.$$

East–west

$F_E \quad F_W \qquad T_p$

Here the left-hand side denotes the rate of change of total energy E, within the Strait, and the various terms on the right-hand side denote the energy generation by the wind, T_w, the loss due to bottom friction, T_b, the outward flux across the eastern end, F_E, and the inward flux at the western end, F_w, and the work done by the east–west pressure gradient, T_p.

Figure 15a shows the term $T_w - T_b$, calculated using conventional expressions for the wind stress (Smith and Banks, 1975) and bottom stress, which is dominated by the wind

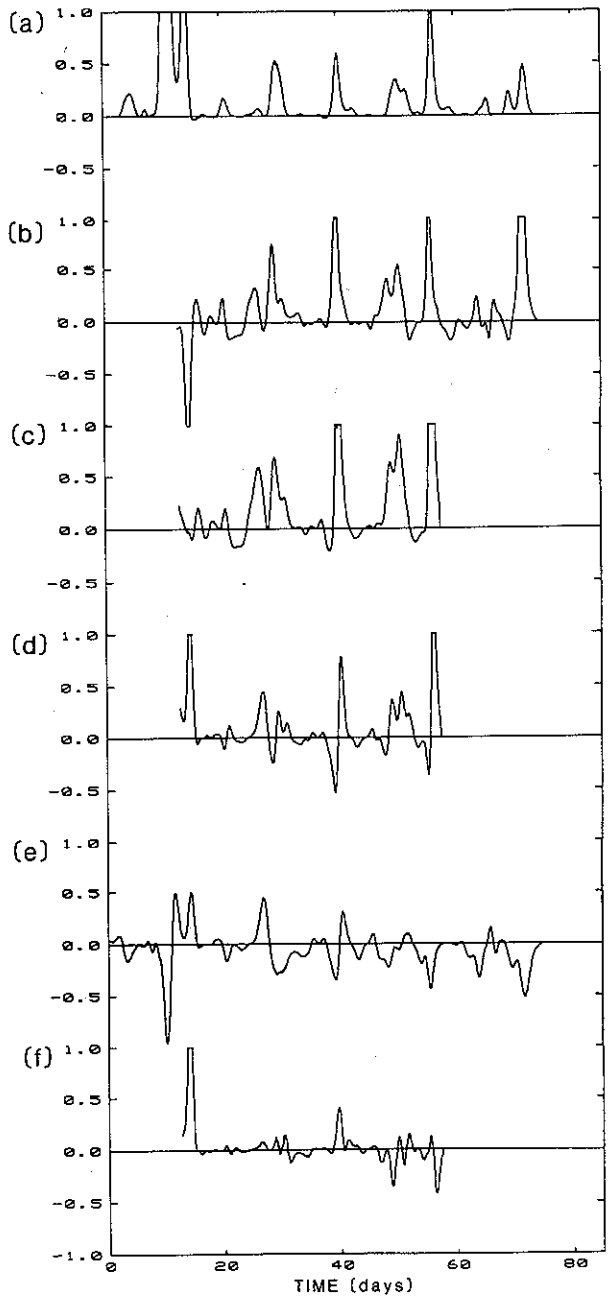

Fig. 15. The variation of the terms of the energy balance equation (20) with time, in normalized units for comparison. (a) The net energy generation rate by wind stress, T_w, minus the loss by bottom stress, T_b, with Bass Strait; (b) eastward energy flux, F_W, across the western boundary; (c) eastward energy flux, F_E, across the eastern boundary; (d) the net loss in energy flux, $F_E - F_W$; (e) the energy generation, T_p, by the atmospheric pressure gradient within Bass Strait; (f) the rate of change of total energy obtained by summing the terms on the right-hand side of equation (20).

stress. The area integral was estimated by using a mean wind, the mass flux of Fig. 6c, and assuming a constant east–west length of 330 km between the two end sections of Cape Otway-Grim and Rabbit Island to Bligh Point. Figure 15b,c shows the eastward energy fluxes across the western, F_w, and eastern, F_E, boundaries, respectively, calculated using the flux curve of Fig. 6c and the mean (over the section) free surface elevations relative to mean sea level. The difference, $F_E - F_w$, is shown in Fig. 15d. The work done by the east–west atmospheric pressure gradient was estimated by multiplying the flux curve of Fig, 6c by the difference in mean atmospheric pressure between the two end sections, η_a (east) $- \eta_a$ (west), and the result is shown in Fig 15e. The net sum of the terms on the right-hand side, with appropriate signs $T_w - T_b + F_w - F_E - T_p$, then gives the rate-of-change term for the energy, $\partial E/\partial t$, and this is shown in Fig. 15f.

We may note first that the residual, $\partial E/\partial t$, is relatively small, so that the right-hand side terms are in approximate balance. This also gives confidence that the estimates of these terms are reasonably accurate. Secondly, the curves for F_w and F_E are similar and are both significantly larger than their difference, d, which is mostly positive. The wind stress, a, almost always acts to increase the energy, E, and the significant peaks coincide with the surges in mass flux in Fig. 7c, whilst the atmospheric pressure gradient term, T_p, has comparable magnitude but is less episodic and may decrease E as well as increase it. This energy generation within Bass Strait will cause an increase in F_E and a decrease in F_w because of Kelvin waves leaving Bass Strait on the northern and southern boundaries, respectively. This energy budget is therefore consistent with the above conclusion that the mass flux through Bass Strait is primarily forced in the region to the west of Bass Strait, with forcing within the Strait playing a secondary role.

7. CONCLUSIONS AND DISCUSSION

We have measured the net flux through Bass Strait over a substantial period during late autumn and winter in 1984. The mean transport during this period was 0.49 Sv from west to east, but it varied between +3.05 and −0.8 Sv. Most of this transport took place in surges lasting 2–3 days which approximately coincided with south-westerly air streams following the passage of atmospheric cold fronts across the region. The flow in these surges was forced by wind stress to the west of Bass Strait and the wind stress in Bass Strait, with these respective contributions being in the approximate ratio of 2:1, based on the semi-quantatitive discussion in Section 6.

Flow through the western gaps is remarkably uniform with latitude except at the southernmost station, where it is significantly larger than elsewhere. As numerical models have shown (FANDRY, 1982), this near uniformity will not be the case throughout Bass Strait. Sea level variations on the Victorian coast bear a remarkable similarity to the observed fluxes through the sections, and this correspondence indicates that any one of these tide gauges could be used to provide an estimate of the total flux, at least in winter periods. The highest correlations are found in the east, and a suitable relationship is provided by equation (19).

A description of the dynamical processes involved has been given in Section 5. In particular, the way in which CTWs are converted (partially) to Kelvin waves as they enter Bass Strait, on the basis of linear theory, has been inferred as part of a process of wave-guide splitting (cf. GILL *et al.*, 1986). The arguments of CLARKE (1987) that the total mass flux is almost entirely due to forcing within Bass Strait are seen to be erroneous, and may

be traced to incorrect mathematical assumptions in his Appendix B. It is also inferred that linear wave theory breaks down in the south-west and the north-east corners of Bass Strait, giving rise to "singularities" of the type described by GILL *et al.* (1986). These singularities should be manifested in strong narrow currents across the shelf-break region, and the strong currents consistently observed at the southernmost mooring may be caused by this behaviour.

With the passage of winter the temperature of the water in Bass Strait progressively decreases. In the west this tends to occur in sudden falls lasting several days and coinciding, roughly, with the surges in current. In the east the temperature decrease is more uniform. We believe that the reasons for this difference are as follows. Winds approaching Bass Strait from the south-west have passed over the relatively colder southern ocean, and are in approximate local thermal equilibrium with it. The progressive cooling of the water column in the Strait due to evaporation and sensible heat loss to the atmosphere will be enhanced during these south-westerly wind surges, and calculations of typical magnitudes of these heat fluxes indicate that they alone may be the sole cause of the sudden falls in temperature in the west. The relative absence of sudden temperature falls in the east is thought to be due to the fact that the atmospheric column will be closer to equilibrium (in both temperature and humidity) with the sea after crossing Bass Strait, than it is in the west. It is also possible (but less likely) that advection of deeper cold water from further west may be important for the temperature falls. BLACKMAN *et al.* (1987) have observed sudden falls in temperature near Black Pyramid (close to the southern section) of 1°C or more, which they attribute to advection of cold water from below 250 m. These large falls were only observed when the water column was stratified and they are usually temporary, apparently because the cold water flows back towards the west. However, Cape Wickham is 80 km (approximately) from the 250 m depth contour, so that a rapid temperature response there due to advection is unlikely.

A number of broader inferences may be made. Firstly, the flux of fluid leaving Bass Strait in the east must be approximately equal to the inflow observed in the western sections, with a time delay of about 5 h (the time taken for a Kelvin wave to cross the Bass Strait). This outflow is believed to occur in the form of an underwater waterfall phenomenon (GODFREY *et al.*, 1986; TOMCZAK, 1985, 1987), particularly in the wintertime, owing to the greater density of the Bass Strait water relative to the surface water further east. On reaching the edge of the continental shelf, the Bass Strait water pours downward over the slope to a depth of about 400 m, where it finds its equilibrium level and passes through a stratified hydraulic jump as it leaves the slope. It then forms an identifiable water mass, which is found throughout the Tasman Sea. The flux in this "underwater waterfall" and the rate of formation of this Tasman Sea water mass must therefore be essentially the same as the flux measured in the experiment described here.

Secondly, these surges in overflow on a time scale of several days may be expected to generate both barotropic and baroclinic CTWs which would propagate northwards along the New South Wales coast. As such, they constitute the probable source for the CTWs observed in the Australian Coastal Experiment (FREELAND *et al.*, 1986) in 1983–1984. This inference is supported by the observation that these waves do not pass around Tasmania (FREELAND *et al.*, 1985; CHURCH and FREELAND, 1987). The differing suggestions by CHURCH and FREELAND and CLARKE (1987) that the waves were generated in the Bight region and within Bass Strait, respectively, seem, therefore to be resolved, with the former predominating by a ratio of approximately 2:1.

Thirdly, the knowledge that currents will be strongest in sympathy with the local wind is useful in determining when bottom stress and sediment movement may be greatest, together with its value for a number of other practical applications associated with oil rigs, fisheries, etc.

Finally, we may note that the weather pattern of south-eastern Australia is dominated by periodic cold fronts throughout the year, and the frontal winds in summer, generally speaking, are similar to those in winter but are less intense. Hence we may speculate that the eastward flux events through Bass Strait will also be dominated by surges lasting 2–3 days throughout the year, but that the mean transport will be reduced or even reversed in summer.

Acknowledgements—Data from the Neil Brown current meters and tide gauges, TG 4–9, were provided by John Church, who in turn obtained the latter from the Tidal Laboratory of the Flinders Institute for Atmospheric and Marine Sciences. The authors are grateful for discussions on the subject with John Church in particular, and also Chris Fandry, Allan Clarke and Bjorn Gjevik, and to Rick Schahinger for comments on the manuscript.

REFERENCES

Baines P. G. and C. B. Fandry (1983) Annual cycle of the density field in Bass Strait. *Australian Journal of Marine and Freshwater Research*, **34**, 143–153.

Blackman D. R., J. B. Hinwood and G. T. Lleonart (1987) Temperature anomaly in western Bass Strait. *Australian Journal of Marine and Freshwater Research*, **38**, 191–195.

Church J. A. and H. J. Freeland (1987) The origin of the Australian Coastal Experiment energy flux. *Journal of Physical Oceanography*, **17**, 289–300.

Clarke A. J. (1987) Origin of the coastally-trapped waves observed during the Australian Coastal Experiment. *Journal of Physical Oceanography*, **17**, 1847–1859.

Easton A. K. (1970) The tides of the continent of Australia. Horace Lamb Centre, Flinders University, South Australia.

Fandry C. B. (1982) A numerical model of the wind-driven transient motion in Bass Strait. *Journal of Geophysical Research*, **87**, 489–517.

Fandry C. B., G. D. Hubbert and P. C. McIntosh (1985) Comparison of predictions of a numerical model and observations of tides in Bass Strait. *Australian Journal of Marine and Freshwater Research*, **36**, 737–752.

Freeland H. J., F. M. Boland, J. A. Church, A. J. Clarke, A. J. M. Forbes, A. Huyer, R. L. Smith, R. O. R. Y. Thompson and N. J. White (1986) The Australian Coastal Experiment: A search for coastal-trapped waves. *Journal of Physical Oceanography*, ***16***, 1230–1249.

Gibbs C. F., R. A. Cowdell and A. R. Longmore (1986) Seasonal variations of density patterns in relation to the Bass Strait cascade. *Australian Journal of Marine and Freshwater Research*, **37**, 21–25.

Gill A. E. (1982) *Atmosphere–Ocean Dynamics*. Academic Press, New York, 662 pp.

Gill A. E., M. K. Davey, E. R. Johnson and P. F. Linden (1986) Rossby adjustment over a step. *Journal of Marine Research*, **44**, 713–738.

Godfrey J. S., I. S. F. Jones, J. G. H. Maxwell and B. D. Scott (1980) On the winter cascade from Bass Strait into the Tasman Sea. *Australian Journal of Marine and Freshwater Research*, **31**, 275–286.

Kundu P. K., J. S. Allen and R. L. Smith (1975) Modal decomposition of the velocity field near the Oregon coast. *Journal of Physical Oceanography* **5**, 683–704.

Longuet-Higgens M. S. (1985) On the trapping of waves along a discontinuity of depth in a rotating ocean. *Journal of Fluid Mechanics*, **31**, 417–434.

Newell B. S. (1961) Hydrology of South-eastern Australian Waters: Bass Strait and New South Wales tuna fishing area. CSIRO Division of Fishery and Oceanography Technical Paper No. 10, 22 pp.

Provis D. G. and R. Radok (1979) Sea level oscillations along the Australian coast. *Australian Journal of Marine and Freshwater Research*, **30**, 295–301.

Smith S. D. and E. G. Banke (1975) Variation of the sea surface drag coefficient with wind speed. *Quarterly Journal of the Royal Meteorological Society*, **101**, 665–673.

Thompson R. O. R. Y (1983) Low-pass filters to suppress inertial and tidal frequencies. *Journal of Physical Oceanography*, **13**, 1077–83.

Tomczak M. Jr (1985) The Bass Strait water cascade during winter 1981. *Continental Shelf Research*, **4**, 255–278.

Tomczak M. Jr (1987) The Bass Strait water cascade during summer 1981–1982. *Continental Shelf Research*, **7**, 561–572.